

Design and construction of the SuperKEKB vacuum system

Yusuke Suetsugu, Ken-ichi Kanazawa, Kyo Shibata, Takuya Ishibashi, Hiromi Hisamatsu et al.

Citation: *J. Vac. Sci. Technol. A* **30**, 031602 (2012); doi: 10.1116/1.3696683

View online: <http://dx.doi.org/10.1116/1.3696683>

View Table of Contents: <http://avspublications.org/resource/1/JVTAD6/v30/i3>

Published by the AVS: Science & Technology of Materials, Interfaces, and Processing

Related Articles

Vacuum frequency mixer with a field emitter array

J. Vac. Sci. Technol. B **31**, 050601 (2013)

Development of planar x-ray source using gated carbon nanotube emitter

J. Vac. Sci. Technol. B **31**, 02B110 (2013)

Tungstate formation in a model scandate thermionic cathode

J. Vac. Sci. Technol. B **31**, 011210 (2013)

Influence of gun design on Coulomb interactions in a field emission gun

J. Vac. Sci. Technol. B **29**, 06F605 (2011)

Model scandate cathodes investigated by thermionic-emission microscopy

J. Vac. Sci. Technol. B **29**, 04E102 (2011)

Additional information on *J. Vac. Sci. Technol. A*

Journal Homepage: <http://avspublications.org/jvsta>

Journal Information: http://avspublications.org/jvsta/about/about_the_journal

Top downloads: http://avspublications.org/jvsta/top_20_most_downloaded

Information for Authors: http://avspublications.org/jvsta/authors/information_for_contributors

ADVERTISEMENT

Instruments for advanced science

Gas Analysis




- dynamic measurement of reaction gas streams
- catalysis and thermal analysis
- molecular beam studies
- dissolved species probes
- fermentation, environmental and ecological studies

Surface Science



- UHV TPD
- SIMS
- end point detection in ion beam etch
- elemental imaging - surface mapping

Plasma Diagnostics



- plasma source characterization
- etch and deposition process reaction kinetic studies
- analysis of neutral and radical species

Vacuum Analysis



- partial pressure measurement and control of process gases
- reactive sputter process control
- vacuum diagnostics
- vacuum coating process monitoring

contact Hiden Analytical for further details

HIDEN ANALYTICAL

info@hideninc.com
www.HidenAnalytical.com

CLICK to view our product catalogue 

Design and construction of the SuperKEKB vacuum system

Yusuke Suetsugu,^{a)} Ken-ichi Kanazawa, Kyo Shibata, Takuya Ishibashi, Hiromi Hisamatsu, Mitsuru Shirai, and Shinji Terui

High Energy Accelerator Research Organization (KEK), Tsukuba, Ibaraki 305-0801, Japan

(Received 25 November 2011; accepted 4 March 2012; published 23 March 2012)

A two-ring electron-positron collider with asymmetric energies—called the SuperKEKB—has been designed by the High Energy Accelerator Research Organization (KEK) as an upgrade of the KEKB B-factory (KEKB), which completed 12 years of operation in 2010. It is anticipated that the SuperKEKB will reach a luminosity of $8 \times 10^{35} \text{ cm}^{-2} \text{ s}^{-1}$, which is approximately 40 times larger than that of the original KEKB. The upgrade of the vacuum system is a key factor that will allow the SuperKEKB to achieve unprecedented high performance. Most of the beam pipes, especially in the positron ring, are newly manufactured to manage the electron cloud effect, and to reduce beam impedance, which is essential to keep the low-emittance beam stable. Our design of the vacuum system implements recent technologies and draws on various experiences and studies during the operation of the original KEKB. The basic design is near completion, and manufacturing of beam pipes and the major vacuum components, such as bellows chambers, gate valves and supports, are in progress. The installation of these components will start in 2013 with the aim of commissioning the SuperKEKB in 2014. © 2012 American Vacuum Society. [<http://dx.doi.org/10.1116/1.3696683>]

I. INTRODUCTION

The KEKB B-Factory (KEKB) is an electron-positron collider developed by the KEK to search for CP violation in the B-meson scheme.¹ The operation of KEKB began in 1998 and finished last year, 2010.² During these 12 years of operation, KEKB recorded a world record for luminosity at $2.1 \times 10^{34} \text{ cm}^{-1} \text{ s}^{-1}$, and experimentally proved the CP violation of B and anti-B mesons predicted by Kobayashi and Masakawa (recipients of the 2008 Nobel Prize in Physics). Now a project to upgrade the KEKB is underway.³ It is anticipated that the upgraded SuperKEKB will reach a luminosity of $8 \times 10^{35} \text{ cm}^{-1} \text{ s}^{-1}$, which is approximately 40 times higher than that of the KEKB, and allow researchers to investigate physics beyond the present standard model.

The main ring of the SuperKEKB consists of two rings, each with a circumference of 3016 m. These serve as the high energy ring (HER) for 7.0 GeV electrons and the low energy ring (LER) for 4.0 GeV positrons.³ The tunnel of the KEKB is to be reused for the SuperKEKB. The schematic layout of the SuperKEKB at the KEK Tsukuba site is shown in Fig. 1. The key parameters of the main ring are listed in Table I. The design beam currents are 2.6 and 3.6 A for the HER and LER, respectively, with a maximum bunch number of 2500. As well as these increases in beam currents compared to the KEKB, the beams in the SuperKEKB design have a very low emittance (8.6–11.5 pm in the vertical direction), and the vertical beam sizes at the collision point have been reduced to approximately 50–60 nm in the vertical direction. In order to meet these challenging beam parameters, the whole accelerator system is being upgraded to cope with various issues and the vacuum system is no exception.

The vacuum system for the SuperKEKB has been designed based on various experiences obtained during the operation of the KEKB,⁴ while also introducing leading-

edge concepts. The main parameters related to the vacuum system are also listed in Table I. The first major issue for the vacuum system stems from the high beam currents. The synchrotron radiation (SR) power and the photon density are consequently high, and the resultant heat and gas loads are also large. The second issue comes from the high bunch current (1.4–1.1 mA per bunch) and the short bunch length (5–6 mm). Higher order modes (HOMs) are likely to be excited as a result, and the beam impedance of various vacuum components needs to be minimized to keep the beam stable and also to avoid excess heating of components. The third and most serious issue is the electron cloud effect (ECE) in the LER.⁵ More rigorous countermeasures than before are required to reduce the electron density in the beam pipe. Otherwise, a single-bunch instability may be excited and the luminosity will deteriorate considerably. Research and development on these issues were performed using the KEKB, and in the SuperKEKB, both newly developed countermeasures and conventional ones will be adopted.

In the following, the design of the vacuum system for the SuperKEKB is described with a focus on the arc sections of the LER, which is a major component of the upgrade. The vacuum system for the HER will be reused as is. Finally, the present status of the upgrade is reported.

II. DESIGN OF VACUUM SYSTEM

A. Beam pipe

One ring consists of approximately 1000 beam pipes, which are each 3–5 m in length. The new beam pipes for the LER arc sections consist of a circular beam channel and two rectangular antechambers on each side (we call this the antechamber scheme).^{6,7} A schematic drawing of a beam pipe for the arc sections is shown in Fig. 2. The beam goes through a beam channel at the center, and the SR passes through an antechamber located outside the ring (SR channel) and hits

^{a)}Electronic mail: yusuke.suetsugu@kek.jp



FIG. 1. (Color online) Schematic layout of the SuperKEKB in the KEK Tsukuba campus.

the side wall of the antechamber. The diameter of the beam channel and the half width at the horizontal plane are 90 and 110 mm, respectively. Main vacuum pumps are situated in an antechamber (pump channel) inside the ring (see Sec. II B). The pump channel is connected to the beam channel through a screen with many small holes. For the wiggler section, where the SR hits both sides of the beam pipe, both antechambers function as SR channels. Two cooling channels are provided on the outside of the antechambers.

Generally, a beam pipe with a larger aperture is better for vacuum evacuation, because the conductance increases with the aperture size. The impedance of the beam pipe is relatively small for large apertures. The aperture of beam pipes; however, is usually limited by the cores of magnets, such as bending magnets, quadrupole magnets, and sextupole magnets. Furthermore, an almost circular beam channel is preferable to minimize the incoherent tune shift due to the resistive wall.⁸ The cross-section of the beam pipe, shown in Fig. 2, fits the presently used magnets and makes the most of the limited space. Note that the coherent synchrotron radiation (CSR) effect requires a small aperture in order to utilize

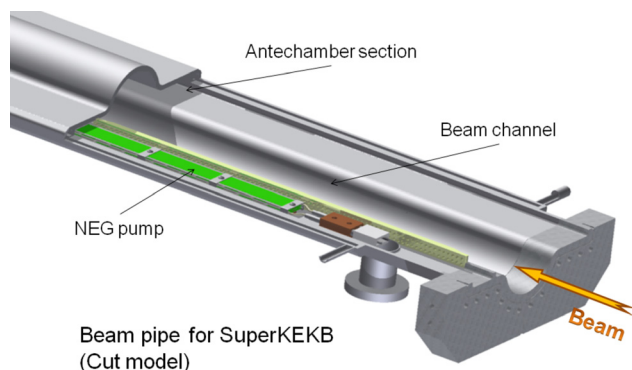


FIG. 2. (Color online) Schematic drawing of a beam pipe for the arc sections of the LER.

the shield effect of the beam pipes.⁹ The bunch lengthening due to the CSR effect; however, was found to be in a tolerable range for the present aperture.¹⁰

The first advantage of the antechamber scheme is that a low beam impedance can be realized. For the cross-section presented in Fig. 2, the electric field accompanied by a bunch is orders of magnitude smaller in the antechamber than in the beam channel, due to the narrow height of the antechamber. Therefore, the pumping ports in an antechamber and the screen in the pump channel have a small beam impedance. Photon masks, which are usually placed downstream of the beam pipe to protect the following flanges and bellows chambers from SR, also have little effect on the beam if placed in the antechamber. Naturally, the cross-section of the beam pipe is kept as uniform as possible to lower the beam impedance.

The second advantage of the antechamber scheme is that the power density of the SR can be reduced because of its vertical and horizontal spread. That is because the incident point of SR on the side wall is far from the point of emission. For the LER arc section, the maximum SR power density (line density) is approximately 2.3 kW m^{-1} (2.2 W mm^{-2}) at a beam current of 3.6 A for a beam pipe with a half-width of 110 mm. For the arc section, aluminum-alloy beam pipes are used as they are readily available. Aluminum-alloy (A6063-T6) beam pipes with antechambers can be formed by an extrusion method. No lead shield is required for the present beam parameters even for aluminum-alloy. The wiggler section in the LER also required this antechamber scheme to reduce the SR power density down to 14 kW m^{-1} (3 W mm^{-2}). Oxygen free copper (OFC) is a suitable material in these cases. The SR power increases up to approximately 50 kW m^{-1} (9 W mm^{-2}) at the SR mask, which blocks the SR to create shadows downstream. The SR masks are made of copper-chrome alloy (CrCu, C18200). No lead shielding is required for copper.

As described above, the beam pipe for the KEKB HER (a race-track shape with a half width of 52 mm) will simply be reused in the SuperKEKB as it is. In the case of the HER, the maximum SR power density (line density) at a beam current of 2.6 A is approximately 8 kW m^{-1} (17 W mm^{-2}), approximately the same as that of the KEKB HER (8 GeV, 1.4 A). This is because the increase in the beam current compensates for the reduction in the beam energy. The beam pipes for the HER are made of OFC because of the high SR power density and radiation shielding. In the future, beam pipes with antechambers will also be proposed for the HER due to the issues associated with SR power, beam impedance, and incoherent tune shifts. If an antechamber structure with a horizontal half-width of 90 mm is used; for example, the SR power density can be reduced to 13 W mm^{-2} at the designed beam current.

Furthermore, the antechamber scheme for the LER helps to minimize photoelectron effects because the emission points of the photoelectrons are far from the beam orbit. As described later in Sec. II C, this is essential in order to reduce ECE.⁵

Several trial models of copper beam pipes with antechambers had been fabricated and installed into the KEKB LER to examine their properties using real beams. The temperatures and vacuum pressures around the beam pipes were monitored during beam operation with a beam current up to 1.6 A (1585 bunches). The copper beam pipes were also installed into a wiggler section ($\sim 30 \text{ m}$), together with bellows chambers and beam position monitors described later. Although it was still within an acceptable range, the temperature of the stainless-steel flanges was high due to Joule heating of the stainless-steel surface. The effect of the antechamber design on the number of photoelectrons was studied, and a reduction in the number of photoelectrons by one or two orders of magnitude compared to a simple circular pipe was confirmed in a low beam-current region.

Since the SuperKEKB operates with a short bunch length and a high bunch current, even gaps or steps at the connection flanges of beam pipes can be a measurable impedance source because the number of flanges are large, although the individual contributions may be small.¹¹ The Matsumoto–Ohtsuka-type (MO-type) flange can seal a vacuum at the inner surface to maintain a smooth current flow across a metal gasket,^{12,13} and provide much smoother connection than flanges with conventional fingers or metal O-rings.^{14,15} A copper alloy (CrCu, C18200) and an aluminum alloy (A2219-T851) flange have been developed instead of stainless steel. This simplifies the manufacturing process of the beam pipes and also reduces Joule loss associated with heating the flange, which was observed in beam tests. A vacuum seal is achieved with a fastening torque less than 18 Nm per bolt, similar to the case of a standard circular flange with the same diameter. The gaskets are made of annealed OFHC or aluminum alloy (A5052-H34).

The beam position monitor (BPM) is a component that measures the beam orbit, and is embedded within the beam pipes for quadrupole magnets. The BPM calculates the beam orbit from the induced fields at four pickup electrodes, which are attached to a block with the same cross-section as the

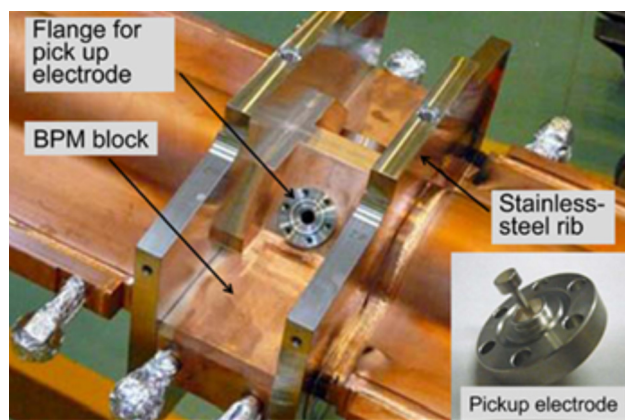


FIG. 3. (Color online) Beam position monitor (BPM) for a beam pipe with antechambers in a wiggler section.

beam pipe. The newly developed BPM for the beam pipe with antechambers is presented in Fig. 3.⁶ The inset shows a pickup electrode. The copper BPM block was reinforced by two stainless-steel ribs. Alternatively, the aluminum BPM block together with ribs is machined from a single block. The pickup electrodes are attached to the block by a UHV flange (ICF034) with a helicoflex-delta seal (Garlock Helicoflex). The final detailed calibration of the BPM will be performed using a circulating beam (i.e., the beam-based alignment).

Because getters are used as the main pump, as described in the next section, the reduction of gas desorption is important to avoid frequent conditioning of the getters and to prolong their life. A chemical polishing procedure; therefore, has been adopted to remove the initial oxide surface including a carbon compound. For copper beam pipes, after degreasing with Na_3PO_4 , the surface was etched with a mixture of H_2SO_4 , H_2O_2 , and isopropanol. For aluminum beam pipes, after degreasing with alcohol, the inner surface was etched with NaOH and brightened with HNO_3 , and then cleansed with an alkali detergent. Finally, the surface of both types of pipes was washed with deionized water and dried with dry nitrogen. Beam pipes will be baked at 150°C for 24 h and the desorption rate will be checked before installing into the ring, as was done during construction of the KEKB.¹⁶ The sputter ion pumps are baked at 250°C to remove water on the cathode surface while in the ring.

B. Pump system

The target vacuum pressure in the ring is on the order of 10^{-7} Pa on average at the designed beam current. This guarantees that a beam lifetime, determined by the vacuum pressure (mostly Bremsstrahlung), is longer than the luminosity life time and is sufficiently long to be compatible with the injection scheme. In order to minimize ion instabilities in the HER, a pressure on the order of 10^{-7} Pa is also required, on average; however, the pressure should be less than 10^{-6} Pa locally. A pressure on the order of 10^{-8} Pa is required near the collision points to decrease background noise, especially upstream of the Belle-II detector.

The main process of gas desorption in beam operation is photodesorption, i.e., desorption caused by SR. In order to

achieve the required pressures described above, a linear pumping speed of approximately $0.1 \text{ m}^3 \text{ s}^{-1} \text{ m}^{-1}$ is required if we assume a photodesorption coefficient (η) of 1×10^{-6} molecules photon^{-1} . In the KEKB, η was found to have decreased with the beam dose down to less than 1×10^{-6} molecules photon^{-1} .¹⁷ In order to effectively evacuate the long, narrow beam pipes, which have a limited conductance, a distributed pumping scheme using a strip-type nonevaporable getter (NEG), ST707 (SAES GETTERS Co., Ltd.) is adopted as the main pump in the LER. A strip-type NEG can be used irrespective of the presence of magnetic fields.^{18,19} Cartridge-type lumped NEGs are also used for the straight section as necessary. Note that NEG-coated beam pipes, which create pumping action to the inner surface, have recently been used in several accelerators.²⁰ However, the small absorbing capacity of the coating can be a problem for relatively high gas-loaded machines.²¹ Furthermore, the low gas desorption rate of the NEG coating is not effective if the aperture has a complicated structure because it is difficult to ensure a uniform coating. The pumping system for the HER is the same as that used in the KEKB. The main pump is also a NEG-type pump, but the pumping scheme is a combination of strip types for beam pipes in bending magnets and lumped cartridge-type NEGs for other parts.⁴

For straight sections, where the SR hits both side walls of the beam pipe, the pump ports are placed on the bottom of the antechambers. For arc sections; on the other hand, the SR hits only the outside of the ring. Therefore, antechambers located on the inside of the ring can be effectively used as a pump channel in the arc section of the LER (see Fig. 2). A screen with many holes of 4 mm diameter that shields the pump from the beam is installed in the antechamber between the pump and the beam. The thickness of the screen is 5 mm, and the conductance is approximately $0.2 \text{ m}^3 \text{ s}^{-1}$ per 1 m.

A pump assembly using multilayered NEG strips for an antechamber space was recently designed, as shown in Fig. 4.²² The number of NEG strips was optimized by calculating the pressure distribution inside the pump channel; as a result, three strips were used. Indirect heating with sheath heaters was considered instead of direct Joule heating in

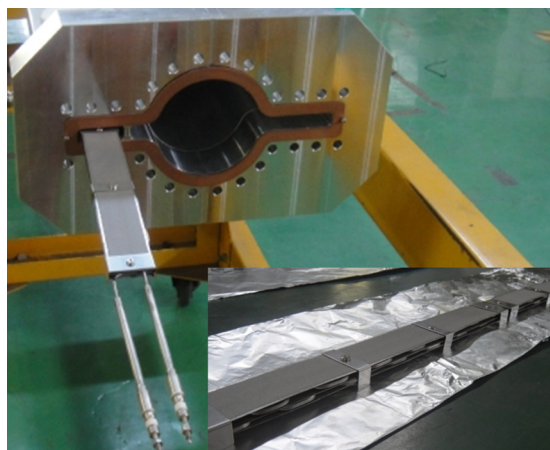


Fig. 4. (Color online) Multilayered NEG strips for the antechamber.

order to safely activate the NEG strips in the narrow space. A pump assembly consisted of several modules of NEG strips, each approximately 300 mm in length, which easily followed the curvature of the bent beam pipe and the change in length caused by thermal expansion during the NEG activation. The total length of the assemblies to be fitted within the beam pipes ranged from 0.6 to 2.7 m. The effect of sheath heaters on the magnetic field was checked using a real bending magnet, and found to be negligible. The effective area of the NEG surface in an assembly is approximately 0.1 m^2 per 1 m.²² The linear pumping speed of the assembly for nitrogen (N_2) just after an activation was approximately $0.2 \text{ m}^3 \text{ s}^{-1} \text{ m}^{-1}$ (i.e., $2.0 \text{ m}^3 \text{ s}^{-1} \text{ m}^{-2}$ for the NEG surface). Therefore, according to the data in the ST707 Catalogue,²³ the pumping speed for carbon monoxide (CO), which is a main gas component in the photodesorption process, was expected to be approximately $2.0 \text{ m}^3 \text{ s}^{-1} \text{ m}^{-1}$ (i.e., $20 \text{ m}^3 \text{ s}^{-1} \text{ m}^{-2}$ for the NEG surface) just after an activation. The combined linear pumping speed expected with a screen is; therefore, approximately 0.1 and $0.18 \text{ m}^3 \text{ s}^{-1} \text{ m}^{-1}$ for N_2 and CO, respectively. If gaps between the NEG assemblies and the length of the bellows chambers are taken into account (approximately 20% in the ring), the effective linear pumping speed along the beam pipe is approximately 0.08 and $0.14 \text{ m}^3 \text{ s}^{-1} \text{ m}^{-1}$ for N_2 and CO, respectively.

Here the frequency of the NEG activation at a steady state is roughly estimated, assuming an η of 1×10^{-6} molecules photon^{-1} . Since the linear photon density at a full current is approximately 5.3×10^{18} photons $\text{s}^{-1} \text{ m}^{-1}$ (see Table I, the gas desorption rate is $2.2 \times 10^{-8} \text{ Pa m}^3 \text{ s}^{-1} \text{ m}^{-1}$ (300 K). If the main gas component is CO, the pressure just after an activation is then approximately $1.6 \times 10^{-7} \text{ Pa}$. The timing of the re-activation will be determined by the beam life time, the background to the detector, and so on. Here we assume that the NEG is activated when the pressure goes up to $1.0 \times 10^{-6} \text{ Pa}$, where the beam lifetime determined by the gas scattering is still longer than that determined by the dynamic beam aperture. In this pressure, the effective linear pumping speed along the beam pipe is approximately $0.022 \text{ m}^3 \text{ s}^{-1} \text{ m}^{-1}$, that is, the pumping speed for the NEG surface is approximately $0.32 \text{ m}^3 \text{ s}^{-1} \text{ m}^{-2}$. From the data in the ST707 Catalogue, the absorbed gas quantity giving this pumping speed is approximately $0.5 \text{ Pa m}^3 \text{ m}^{-2}$ for the NEG surface, that is, $0.04 \text{ Pa m}^3 \text{ m}^{-1}$ along the beam pipe. Therefore, the interval between activations are approximately $1.8 \times 10^6 \text{ s} = 21$ days. Activation will be required approximately every month for continuous full-current operation.

To evacuate nonactive gases and to enable more efficient evacuation in relatively high pressure regimes, sputter ion pumps with a pumping speed of $0.2 \text{ m}^3 \text{ s}^{-1}$ at 10^{-8} Pa are provided as an auxiliary pump and positioned approximately every 10 m along the ring. The rough pumping system, which is used for the evacuation near atmospheric pressure regime, is completely oil-free and is based on a turbomolecular pump ($0.2 \text{ m}^3 \text{ s}^{-1}$) and a scroll-style dry pump ($250 \text{ m}^3 \text{ min}^{-1}$). A rough pumping port is located every 40 m along the ring.

TABLE I. Main parameters of the SuperKEKB and vacuum system.

	LER (positron)	HER (electron)	Unit
Beam energy	4.0	7.0	GeV
Beam current	3.6	2.6	A
Circumference		3016	m
Number of bunches		2500	
Bunch current	1.44	1.06	mA
Bunch length	6.0	5.0	mm
ϵ_x/ϵ_y	3.2/8.64	4.6/11.5	nm/pm
β_x^*/β_y^*	32/0.27	25/0.3	mm
Crossing angle		83	mrad
Luminosity		8×10^{35}	$\text{cm}^{-1} \text{s}^{-1}$
Bending radius	74.68 (arc)	104.46 (arc)	m
	15.48 (wiggler)	45.52 (wiggler)	
Beam pipe material	Al (arc)	OFC (arc),	
	OFC (wiggler)	OFC (wiggler)	
Cross section of beam pipe	Circle (ϕ 90) + Antechamber	Racetrack (50×104) Circle (ϕ 90) + Antechamber	
Main pumps	NEG (strip)	NEG (strip + cartridge)	
Total power of SR ^a	1.1 (arc)	5.3 (arc)	MW
	6.3 (wiggler)	1.8 (wiggler)	
Critical energy of SR	1.9 (arc)	7.3 (arc)	keV
	9.2 (wiggler)	17 (wiggler)	
Total photon flux of SR	1.2×10^{22} (arc)	1.5×10^{22} (arc)	photons s^{-1}
	1.4×10^{22} (wiggler)	2.1×10^{21} (wiggler)	
Max. linear power density of SR	2.3 (arc)	8.1 (arc)	kW m^{-1}
	14 (wiggler)	10 (wiggler)	
Avg. linear photon density	$\sim 5.3 \times 10^{18}$ (arc)	$\sim 6.7 \times 10^{18}$ (arc)	photons $\text{s}^{-1} \text{m}^{-1}$
	$\sim 4.7 \times 10^{19}$ (wiggler)	$\sim 2.1 \times 10^{19}$ (wiggler)	
Linear pumping speed	~ 0.1 (arc)	~ 0.06 (arc)	$\text{m}^3 \text{s}^{-1} \text{m}^{-1}$
Arrange of pump	Integrated + port	Integrated + port	
	port	port	
Ave. pressure with beam		$\sim 10^{-7b}$	Pa
Ave. base pressure		$\sim 10^{-8}$	Pa
Static desorption rate		$< 10^{-8}$	$\text{Pa m}^3 \text{s}^{-1} \text{m}^{-2}$

^aSynchrotron radiation.

^b η of 1×10^{-6} molecules photon⁻¹ is assumed.

C. Countermeasures for the electron cloud effect

The ECE has been a critical issue in recent high-intensity positron/proton rings.^{5,24} The single-bunch instability caused by the electron cloud presents a serious problem for the SuperKEKB, and more thorough countermeasures than ever before are required.²⁵ From a simulation, the average electron density in the beam pipe should be less than approximately 1×10^{11} electrons m^{-3} .

The electron cloud is initially created by photoelectrons emitted from the surface being irradiated by SR. The antechamber scheme; therefore, helps to minimize the effects of the photoelectrons because their emission points, which are on the side walls, are far from the beam orbit, and the attractive electric field induced by the beam is weak. Furthermore, the surface of the side wall will be roughened to a roughness (Ra) between 7 and 20 μm to suppress photon scattering.

In a high bunch current regime; however, secondary electrons due to electron impact play a major role in forming the electron cloud. The electron density increases by a chain of

electron emissions, that is, by multipactoring.²⁶ Actually, in the experiment at the KEKB, the electron density in the antechamber at a high beam current region was reduced to approximately 1/5 compared to the case of a circular beam pipe, although that at a low beam current was reduced to approximately 1/100.

A solenoid field is very effective at preventing multipactoring, and was successfully used at the KEKB.^{27,28} It was found that the electron density around a beam decreased by several orders of magnitude when the solenoid field was applied to a circular copper beam pipe.²⁹ Considering the gaps between the adjacent solenoids and the regions for the polarity change, the reduction efficiency in the electron density was actually expected to be approximately 1/50 for the solenoid.

The solenoid method; however, is available only in drift regions (field-free regions) of the ring. Another way to suppress the secondary electron emission is to coat the inner surface with materials that have a low secondary electron yield

(SEY), such as titanium nitride (TiN), NEG, or graphite. These coatings can be used in drift regions and also inside magnets. A TiN coating has been used in the LER beam pipes of PEP-II³⁰ and the coating technique is well developed. It should be noted that a bare aluminum alloy has a much higher SEY than copper and any coatings are indispensable.²⁴

Circular copper chambers with NEG or TiN coatings were installed in the arc and straight sections of the KEKB LER for tests, and the number of electrons around the positron beams was measured and compared.³¹ In the experiment, the electron numbers in the beam pipes with the TiN coating and the NEG coating were approximately 1/3 and 2/3 of that for a copper chamber without any coating in the straight section where little SR was irradiated and the effect of photoelectrons was small. The TiN coating showed a similar result on an aluminum test chamber. The TiN coating seemed to be the most promising coating. After a sufficient aging process, a SEY of approximately 1.0 is expected for the TiN coating.²⁴

The thin TiN is usually coated by a sputtering of Ti rod using a magnetron discharge in an Ar and N₂ atmosphere. Various conditions during the magnetron sputtering, such as pressure, temperature, and magnetic field, had been investigated in a laboratory.³² As a result, it was concluded that the optimum film had a thickness of 0.2 μm and was applied to a substrate with a temperature of 150 C. For a beam pipe with antechambers, a cathode rod (Ti) was installed along the beam channel, and then the coating was formed mainly on the inner surface of the beam channel. Most of the beam pipes for the LER will be coated using a new facility at KEK.

It was reported recently that a grooved surface and a clearing electrode can be very useful, as they suppress the electron cloud, especially in a dipole-type field, such as a bending magnet and a wiggler magnet.^{24,33-41} The grooved surface reduces the SEY geometrically, and the clearing electrode absorbs the electrons around the beam orbit due to a static electric field. The SuperKEKB has long wiggler sections (~ 150 m) and about 100 bending magnets (~ 520 m). Considering the relatively high electron density in the dipole field,²⁴ a reduction in the electron density in these regions is essential.

Triangular-type groove surfaces with varying geometrical parameters (such as the angle of the triangles, the tip roundness and the pitch of the grooves) and surface conditions (i.e., with or without TiN coating) have been investigated in a wiggler magnet of the KEKB LER and also in the laboratory (magnetic field free).³⁷ It was found that they can reduce the electron density by several multiples compared to that for a plain stainless-steel surface. The sharper the tip and the smaller the tip roundness, the more prominent the reduction. The TiN coating on the grooves enhanced reduction of electron density. A reduction in electron density by the use of grooved surfaces has also been experimentally demonstrated in CESR-TA, at Cornell University.³⁸ In our SuperKEKB design, the grooved surface is adopted for beam pipes in the bending magnets in the arc sections. A schematic drawing of

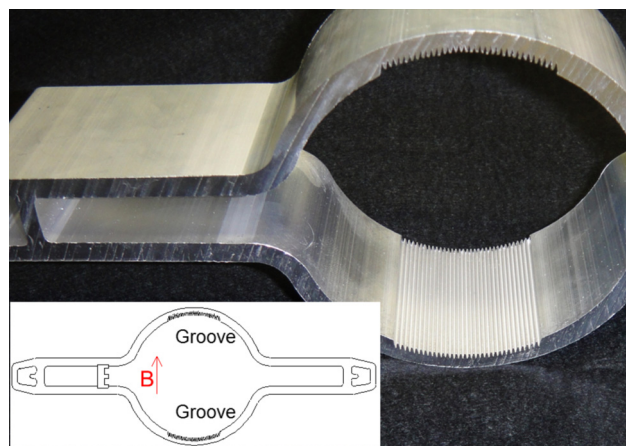


FIG. 5. (Color online) Cut sample and the cross-section of a beam pipe with groove structures for the LER bending magnet.

an aluminum-alloy beam pipe and the cross-section with a grooved surface is presented in Fig. 5. The groove is a triangle type where a tip has an angle of approximately 20 and a roundness of approximately 0.1 mm. The beam pipe with grooves, shown in Fig. 5, was made using an extrusion method. The TiN film is subsequently applied to the grooved surface.

The clearing electrode is not a novel idea and has previously been applied to proton rings.³⁹ The high beam impedance; however, has made it difficult to apply the method to recently established high-intensity positron/proton rings. A method for forming a thin electrode on an inner surface using a thermal spray was developed at KEK.⁴¹ The electrode has a total thickness of approximately 0.3 mm (multiple layers of 0.2 mm aluminum ceramics and 0.1 mm of tungsten on the aluminum layer) and has a low beam impedance and a high thermal conductivity to the beam pipe compared to the conventional strip-line type. The electrode was installed into a wiggler magnet of the KEKB LER and the electron density was measured. A reduction in the electron density of one or two orders of magnitude was observed when a positive voltage greater than 300 V was applied to the electrode. The present design uses the clearing electrode in a wiggler magnet, where the beam pipe is straight and the thermal spray is easily applied. Figure 6 shows the inside view and the cross-section of the pipe with clearing electrodes. Each electrode has a length of 1.6 m and one feed-through. A positive dc voltage of 500 V will be applied to the electrode during operation. Although the circulating beam sees the ceramic layer around the electrode (a width of approximately 4 mm), no problem was found in the experiment at the KEKB. A clearing electrode with a similar structure was installed into the CESR-TA at Cornell University and the electron density reduction effect in a wiggler magnet was verified.³⁸

The countermeasures against the ECE applied to the main sections in the LER are summarized in Table II. The circles indicate the applied countermeasures in each section. The electron densities expected in the case of circular beam pipes (copper) and those with the above countermeasures are

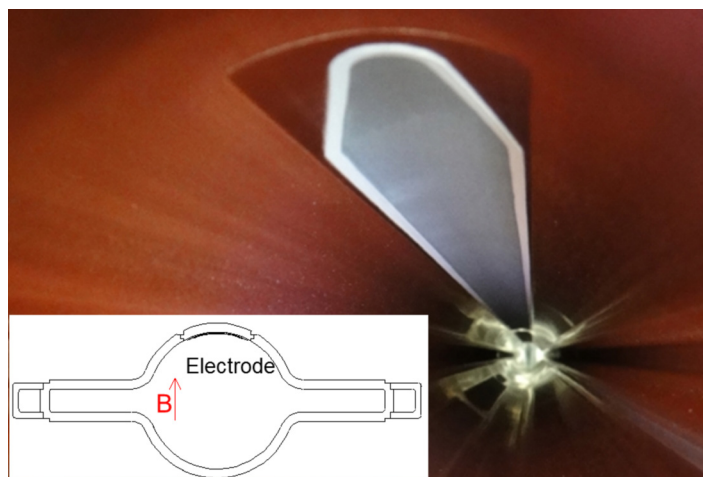


FIG. 6. (Color online) Inside view and the cross-section of a beam pipe with clearing electrodes for the LER wiggler magnet.

presented in the table. Here the reduction efficiency in the electron density for antechamber scheme, TiN coating, solenoid, grooved surface, and clearing electrode are assumed to be 1/5, 3/5, 1/50, 1/2, and 1/100, respectively, based on the experimental results obtained thus far.⁴⁰ Ultimately, an average electron density less than 1×10^{11} (approximately 2×10^{10}) electrons m^{-3} is expected.

For the SuperKEKB, 112 clearing electrodes will be adopted for the wiggler sections. Furthermore, 120 beam pipes with grooved surfaces (4.7 m long) will be installed in the bending magnets in the ring. The contribution of the

grooved structure and the clearing electrode to the total impedance was found to be very small, partially attributable to the relatively large aperture of the beam pipes. The contribution of the loss factors; for example, is less than 1% of the total loss factor in a ring.

D. Key components

Bellows chambers are installed between adjacent beam pipes to ease beam pipe installation and to absorb any thermal deformation. More than 1000 bellows chambers are

TABLE II. Countermeasures used to minimize ECE in the LER. The circular dots indicate the applied countermeasures for each main sections in the ring. Abbreviations—cav. section: beam pipes around RF cavities, IR: interaction region, occ. length: occupied length, n_e (circular): electron density expected for circular beam pipe (copper), n_e (expected): electron density expected after applying countermeasures, ante: antechamber scheme, TiN: TiN coating, sol.: solenoid winding, gr.: beam pipe with grooves, elec.: Beam pipe with clearing electrodes, average: averaged values weighted with the lengths of corresponding sections.

Sections	Length [m]	Occ. length [%]	n_e (circular) [$\text{e}^- \text{m}^{-3}$]	Countermeasures					n_e (expected) [$\text{e}^- \text{m}^{-3}$]	Pipe materials
				Ante (1/5)	TiN (3/5)	Sol. (1/50)	Gr. (1/2)	Elec. (1/100)		
Drift space (arc)	1629	54	8×10^{12}	•	•	•			2×10^{10}	Al (arc)
Corrector mag.	316	10	8×10^{12}	•	•	•			2×10^{10}	Cu (straight) Al (arc)
Bending mag.	519	17	1×10^{12}	•	•		•		6×10^{10}	Al
Wiggler mag.	154	5	4×10^{12}	•	•			•	5×10^9	Cu
Quadrupole and Sextupole mag.	254	9	4×10^{10}	•	•				5×10^9	Al (arc) Cu (straight)
RF cav. section	124	4	1×10^{11}		•	•			1×10^9	Cu
IR	20	1	5×10^{11}		•	•			6×10^9	Cu, Al
Total	3016	100								
Average			5.5×10^{12}						2.4×10^{10}	

used in one ring, and special attention is paid to the reliability of their RF shield. Because the beam current is large and the bunch length is small in the SuperKEKB, the heating of bellows chambers due to the HOM, especially TE-modelike HOM, will become a serious problem. The present design is equipped with a comb-type RF-shield structure that has a higher thermal strength and a lower impedance than previously reported RF-shields.⁴² The RF shield consists of thin, interlocking comb-teeth. It can be used in various cross-sections of the beam pipe, such as a beam pipe with antechambers. The comb-type RF-shield also will be used for approximately 70 gate valves based on the standard design of the VAT Series 47 with RF shield (VAT, INC.). A comb-type RF shield for these components is shown in Fig. 7.

Various types of bellows chambers and gate valves with comb-type RF-shields had been installed into the LER and HER of the KEKB and tested with high-current beams. The bellows chambers and gate valves did not cause problems, such as bursts of vacuum pressure due to arcing. Some bellows chambers with conventional finger-type RF shields were replaced by those with the comb-type, and a reduction in bellows temperature was observed. It was also interesting to note that the temperature of an existing bellows chamber connected to the gate valve with a finger-type RF shield also decreased after the gate valve was replaced with a new comb-type RF shield. This indicated that the excited HOMs decreased when the comb-type RF shield was used.

In order to protect Belle-II from damage due to spent high-energy particles and to reduce the background noise, a movable mask (collimator) system will be installed in each ring.^{43,44} The exact number and location have not been selected yet, but there will be approximately 10 in. each ring. The movable mask will be placed near the circulating beam, and a wide variety of problems should be anticipated and investigated. The first issue is the HOMs generated due to the mask head. A jaw-type movable mask that had been used in PEP-II, which has a trapped-mode-free structure, will be employed in the SuperKEKB during the commissioning stage.⁴⁴ HOM dampers will also be included with the movable mask system. The second problem is the formation of a groove on the mask head by an attack of the circulating

beam when a deviation of the beam orbit occurs. Any material would melt if the entire number of circulating particles hit the mask head. The present design uses tungsten for the mask head because it has a high thermal conductivity, good electrical conductivity, and a high melting point, but it should be designed to be easily replaceable. The third problem is the transverse mode coupling (TMC) instability.⁴⁵ Because the beam size is small, the mask head should be positioned just a few mm from the beam, to function effectively. The transverse impedance becomes large as a result and TMC instability is likely to occur. Detailed tracking simulations of TMC instability are currently being performed. Accurately controlling the position of the mask head presents a mechanical challenge. Fine feedback of the mask head position from the beam orbit will also be required.

E. Monitor and control system

The control and monitoring system design follows that of the KEKB system.⁴⁶ About 300 cold cathode gauges are located approximately 10 m apart in each ring to monitor the total pressure. Several residual gas analyzers are also installed to identify the component of desorbed gas. Vacuum switches are used to detect over-pressure, i.e., pressures higher than 1000 Pa. Approximately 300 wheel-type flow meters monitor the flow rate of cooling water. Temperatures at approximately 6000 points in various vacuum components are monitored by a platinum resistance thermometer sensor (Pt 100, Class B). Furthermore, several photo-electron monitors will be installed in the LER for studying the ECE in the future. All of these monitors will measure and record data every 1 or 2 s. In addition to the usual recording, a rapid recording system that can store data for several minutes will be prepared so that in case an accident occurs, this data can be analyzed to help diagnose the problem.

The vacuum components are controlled by distributed control systems that are based on the Experimental Physics Industrial Control System. They are controlled and monitored using a graphical user interface. The activation of NEG pumps and the position of the movable masks will be controlled remotely from the control room. The old data acquisition system based on the Computer-Aided Measurement And Control System and General Purpose Interface Bus System will be replaced by a new compact system based on Ethernet protocols. Highly reliable alarm and interlock systems are incorporated into the control system. An abnormal increase of any component's temperature or pressures, or a decrease of the flow rate of cooling water results in an alarm and ultimately a beam abort signal.

F. Other subsystems

The cooling power should be improved due to the total SR power being a factor of 2 higher than that of the KEKB. The power loss of both rings is estimated to be approximately 14 MW total (Table I). The cooling capacity of the vacuum system design is only about 8 MW total. Because the dissipation of SR power is concentrated in the wiggler section and the section downstream from this, the location of

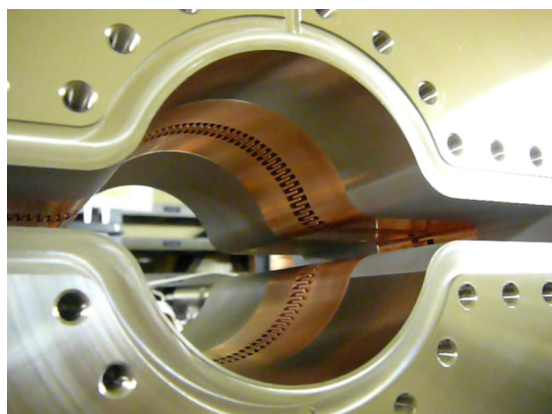


Fig. 7. (Color online) Comb-type RF-shield for gate valves.

cooling facilities and the pipe arrangement should be considered carefully.

The temperature of water is kept at approximately 30 ± 1 C at the entrance of beam pipes. The average flow rate is about $0.01 \text{ m}^3 \text{ min}^{-1}$ along the beam pipe. The length of one cooling loop in the tunnel and the layout of the loop should also be optimized. The main water pipes for the HER and the LER are made of copper and aluminum, respectively, and stainless steel connectors are used to avoid electric erosion. The cooling water is deoxidized pure water.

The compressed air system from the KEKB also will be reused in the SuperKEKB to actuate gate valves. The compressed air is provided by two compressors on the ground. A dry nitrogen system will be prepared to make vacuum system maintenance easier in the tunnel. The nitrogen will be supplied from liquid nitrogen stored in a refrigerator system on the ground. Electric power plugs will be installed in the tunnel for *in situ* rough pumping, welding, and controls.

III. PRESENT STATUS

The KEKB ceased operating in June, 2010. The disassembling of the LER arc section began soon after. Components including the beam pipes, bellows chambers, gate valves, and supports were removed from the tunnel after checking for radioactivity. The components in a local chromaticity correction region, which spans approximately 200 m on either side of a collision point, were also removed for both the LER and HER. Ion pumps and some portions of NEG pumps were reserved for re-use in the SuperKEKB.

The manufacturing of beam pipes and bellows chambers for wiggler sections began in 2010. The straight beam pipes for the wiggler section of the LER have clearing electrodes as described above. A straight beam pipe with two clearing electrodes connected to a beam pipe for a quadrupole magnet is shown in Fig. 8. The baking test of the beam pipe is currently being performed. Although the beam pipe can be baked at up to 120 C, taking into account the thermal expansion of the electrodes, a base pressure on the order of 10^{-8}

Pa was obtained after baking using a turbomolecular pump and NEG pumps.

Approximately 700 aluminum beam pipes for the LER arc section are now being manufactured. A prototype of the beam pipe for a quadrupole magnet is shown in Fig. 9. The flanges and the BPM blocks were machined from blocks, and welded to the beam pipe by TiG welding. The flanges for the NEG heaters are machined from a clad material from aluminum to stainless steel. Copper beam pipes for the downstream side of the wiggler sections and for a chicane section, where the SR power is as high as a wiggler section, are also currently being manufactured. The mass production of these beam pipes will start soon, and they will be completed during this fiscal year. The supports for the beam pipes (approximately 700) and for the ion pumps (approximately 250) are also being manufactured. Approximately 800 bellows chambers and 24 gate valves will also be manufactured.

The beam pipes and the bellows chambers for the HER will be re-used as described above. However, the Tohoku Earthquake on March 11th, 2011, severely damaged the finger-type RF shields of some of approximately 900 bellows chambers. Extra-heating is expected for these bellows chambers during the operating of the SKEKB. The nondestructive inspection of the bellows chambers using x-rays is now being considered.

TiN coating and prebaking facilities are now being prepared in an experimental hall of the ring. There will be five vertical and two horizontal coating apparatuses to complete all of the coating in one and half years. We will have five prebaking apparatuses that blow hot air to heat the beam pipe, which is contained in a thermally insulated box. One apparatus can bake more than two beam pipes at the same time. The baking power and NEG activation during the prebaking process will be controlled via computers.

The optics for the local chromaticity region in the LER and HER are currently being designed. The beam pipes for this region will be designed next year (2013), and will be manufactured as soon as the design is finalized. The beam



Fig. 8. (Color online) Copper beam pipes for wiggler sections.

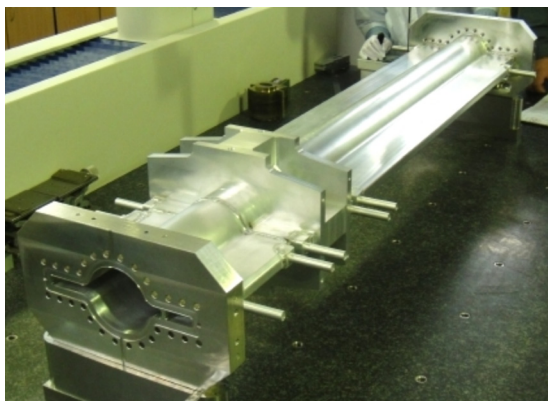


FIG. 9. (Color online) Prototype of an aluminum-alloy beam pipe for the arc sections.

optics in these regions is essential in order to realize the desired luminosity, and special magnets; for example, rotatable skew quadrupole magnets, will be prepared. The beam pipes must be very carefully designed as a result. The beam pipes close to the collision point are also being designed. A prototype of the beam pipes at the collision point will be manufactured next year (2013).

The movable collimator described in Section II.D is an important but difficult component. Brazing tests of tungsten are now being performed, together with design work for the cooling path. The structural design of mask heads and the drive mechanism will be completed in 2012. The first test model will be constructed in 2013, and the type to be used in the SuperKEKB will be prepared just before commissioning begins.

IV. SUMMARY

The SuperKEKB vacuum system design is nearly complete except for the local chromaticity correction region near the collision point. The design was based on experience obtained while the KEKB was operating, and some more recent methods and technological advances have been included, especially for minimizing ECE in the LER. Most of the beam pipes for the arc and wiggler magnet regions are now under construction. Preparation of the TiN coating and prebaking facilities are also in progress. The full-scale installation of beam pipes and components will start in 2012. The Tohoku Earthquake on March 11th, 2011 caused considerable damage to the KEKB facilities, which has created additional work to recover components. The upgrade project; however, is proceeding steadily in spite of these problems.

ACKNOWLEDGMENTS

Sincere thanks are due to the members of the accelerator department of the KEKB for their collaboration. The authors especially thank K. Oide, K. Akai, and H. Koiso for their continuous encouragement during this work.

¹KEK Report No. 95-1, 1995.

²Y. Funakoshi *et al.*, Proceedings of the 2010 International Particle Accelerator Conference, Kyoto, 23–28 June 2010 (unpublished), pp. 2372.

- ³SuperKEKB Task Force, KEK Report No. 2004-4, 2004, <http://www-superkekb.kek.jp/>
- ⁴K. Kanazawa, S. Kato, Y. Suetsugu, H. Hisamatsu, M. Shimamoto, M. Sato, and M. Shirai, *Appl. Surf. Sci.* **169–170**, 715 (2001).
- ⁵K. Ohmi and F. Zimmermann, *Phys. Rev. Lett.* **85**, 3821 (2000).
- ⁶Y. Suetsugu, K. Shibata, H. Hisamatsu, M. Shirai, and K. Kanazawa, *Vacuum* **84**, 694 (2009).
- ⁷D. Hunt, K. Kennedy, and T. Stevens, Proceedings of the 1995 Particle Accelerator Conference, Dallas, 1–5 May, 1995, p. 2067.
- ⁸A. Chao, S. Heifets, and B. Zotter, *Phys. Rev. ST Accel. Beams* **5**, 111001 (2002).
- ⁹T. Agoh and K. Yokoya, *Phys. Rev. ST Accel. Beams* **7**, 054403 (2004).
- ¹⁰K. Oide *et al.*, Proceedings of the 2009 Particle Accelerator Conference, Vancouver, 4–8 May 2009 (unpublished), p. 23.
- ¹¹A. Novokhatski, J. Seeman, and M. Sullivan, Proceedings of the 2008 European Particle Accelerator Conference, Genoa, 23–27 June 2008 (unpublished), p. 1664.
- ¹²Y. Suetsugu *et al.*, *J. Vac. Sci. Technol. A* **27**, 1303 (2009).
- ¹³H. Matsumoto, F. Fukuda, K. Saito, H. Inoue, N. Sakamoto, K. Ueno, and D. Iwai, Proceedings of the 2006 European Particle Accelerator Conference, Edinburgh, 26–30 June 2006 (unpublished), p. 753.
- ¹⁴W. Unterlerchner, *Vacuum* **41**, 1920 (1990).
- ¹⁵J. R. Chen and Y. C. Liu, *Vacuum* **44**, 545 (1993).
- ¹⁶K. Kanazawa, S. Kato, Y. Suetsugu, H. Hisamatsu, M. Shimamoto, M. Sato, and M. Shirai, *Appl. Surf. Sci.* **169–170**, 720 (2001).
- ¹⁷Y. Suetsugu, K. Kanazawa, S. Kato, H. Hisamatsu, M. Shimamoto, and M. Shirai, *J. Vac. Sci. Technol. A* **21**, 1436 (2003).
- ¹⁸C. Benvenuti and F. Francia, *J. Vac. Sci. Technol. A* **8**, 3864 (1990).
- ¹⁹S. Yokouchi, T. Nishidono, Y. Morimoto, H. Daibo, Y. Lee, S. R. In, and S. H. Be, Proceedings of the 1990 European Particle Accelerator Conference, Nice, 12–16 June 1990 (unpublished), p. 1332.
- ²⁰P. Chiggiato and R. Kersevan, *Vacuum* **60**, 67 (2001).
- ²¹C. Benvenuti, P. Chiggiato, P. Costa Pinto, A. Escudeiro Santana, T. Hedley, A. Mongelluzzo, V. Ruzinov, and I. Wevers, *Vacuum* **60**, 57 (2001).
- ²²Y. Suetsugu, K. Shibata, and M. Shirai, *Nucl. Instrum. Methods Phys. Res. A* **597**, 153 (2008).
- ²³Technical specification of “ST707/CTAM/30D Strip (Doc. No. M.F140.0021.21, Rev. 0),” SAES Getters SpA., Italy, 1994.
- ²⁴Reports presented in Mini-Workshop on Electron-Cloud Simulations for Proton and Positron Beams (E-CLOUD’02), CERN, 15–18 April 2002 (unpublished); 31st ICFA Advanced Beam Dynamics Workshop on Electron-Cloud Effects (E-CLOUD’04), Napa, 19–23 April 2004 (unpublished); International Workshop on Electron Cloud Effects (E-CLOUD’07), Daegu, 9–12 April 2007 (unpublished); ECL2 Workshop, CERN, 28 February–2 March 2007 (unpublished); 49th ICFA Advanced Beam Dynamics Workshop on Electron Cloud Physics (E-CLOUD’10), Cornell University, 8–12 October 2010 (unpublished).
- ²⁵H. Jin and K. Ohmi, in 49th ICFA Advanced Beam Dynamics Workshop on Electron Cloud Physics (E-CLOUD’10), Cornell University, 8–12 October 2010 (unpublished).
- ²⁶O. Gröbner, Proceedings of the 10th International Conference on High Energy Accelerators, Protvino, 11–17 July 1997 (unpublished), p. 277.
- ²⁷Y. Funakoshi *et al.*, Proceedings of the 2006 European Particle Accelerator Conference, Edinburgh, 26–30 June 2006 (unpublished), p. 610.
- ²⁸Y. Cai, M. Pivi, and M. Furman, Proceedings of the 2003 Particle Accelerator Conference, Portland, 12–16 May 2003 (unpublished), p. 350.
- ²⁹K. Kanazawa, H. Fukuma, H. Hisamatsu, and Y. Suetsugu, Proceedings of the 2005 Particle Accelerator Conference, Knoxville, 16–20 May 2005 (unpublished), p. 1054.
- ³⁰K. Kennedy, B. Harteneck, G. Millos, M. Benap, F. King, and R. Kirby, Proceedings of the 1997 Particle Accelerator Conference, Vancouver, 12–16 May 1997 (unpublished), p. 3568.
- ³¹Y. Suetsugu, K. Kanazawa, K. Shibata, and H. Hisamatsu, *Nucl. Instrum. Methods Phys. Res. A* **578**, 470 (2007).
- ³²K. Shibata, H. Hisamatsu, K. Kanazawa, Y. Suetsugu, and M. Shirai, Proceedings of the 2008 European Particle Accelerator Conference, Genoa, 23–27 June 2008 (unpublished), p. 1700.
- ³³M. Pivi, F. K. King, R. E. Kirby, T. O. Raubenheimer, G. Stupakov, and F. Le Pimpec, *J. Appl. Phys.* **104**, 104904 (2008).
- ³⁴A. A. Krasnov, *Vacuum* **73**, 195 (2004).
- ³⁵L. F. Wang, D. Raparia, J. Wei, and S. Y. Zhang, *Phys. Rev. ST Accel. Beams* **7**, 034401 (2004).

- ³⁶E. Mahner, T. Kroyer, and F. Caspers, Proceedings of the 2008 European Particle Accelerator Conference, Genoa, 23–27 June 2008 (unpublished), p. 1655.
- ³⁷Y. Suetsugu, H. Fukuma, M. Pivi, and L. Wang, *Nucl. Instrum. Methods Phys Res. A* **604**, 449 (2009).
- ³⁸J. R. Calvey *et al.*, Proceedings of the 2011 International Particle Accelerator Conference, San Sebastián, 4–9 September 2011 (unpublished), p. 796.
- ³⁹S. Bartalucci *et al.*, Proceedings of the 1987 Particle Accelerator Conference, Washington, D.C., 16–19 March 1987 (unpublished), p. 1234.
- ⁴⁰Y. Suetsugu, Presentation in the 49th ICFA Advanced Beam Dynamics Workshop on Electron Cloud Physics (ECLLOUD'10), Cornell University, 8–12 October 2010 (unpublished).
- ⁴¹Y. Suetsugu, H. Fukuma, L. Wang, M. T. F. Pivi, A. Morishige, Y. Suzuki, and M. Tsukamoto, *Nucl. Instrum. Methods Phys. Res. A* **598**, 372 (2009).
- ⁴²Y. Suetsugu *et al.*, *Rev. Sci. Instrum.* **78**, 043302 (2007).
- ⁴³Y. Suetsugu, T. Kageyama, K. Shibata, and T. Sanami, *Nucl. Instrum. Methods Phys Res. A* **513**, 465 (2003).
- ⁴⁴J. Seeman, S. DeBarger, S. Metcalfe, M. Nordby, and C. Ng, Proceedings of the 2000 European Particle Accelerator Conference, Vienna, 26–30 June 2000 (unpublished), p. 2298.
- ⁴⁵A. W. Chao and M. Tigner, *Handbook of Accelerator Physics and Engineering* (World Scientific, Singapore, 1999), p. 119.
- ⁴⁶S. Kato, K. Kanazawa, Y. Suetsugu, H. Hisamatsu, M. Shimamoto, M. Sato, M. Shirai, and M. Takagi, *Appl. Surf. Sci.* **169–170**, 732 (2001).